SUPPORTING INFORMATION

Generation, spectroscopic and chemical characterization of an octahedral iron (V) – nitrido species with a neutral ligand platform

Gerard Sabenya,[a] Laura Lázaro,[a] Ilaria Gamba,[a] Vlad Martin–Diaconescu,[a,*] Erik Andris,[b] Thomas Weyhermüller,[c] Frank Neese,[c*] Jana Roithova,[b,*] Eckhard Bill,[c,*] Julio Lloret–Fillol,*[,d,e] Miquel Costas.*[,a]

a) Grup de Química Bioinorgànica i Supramolecular (QBIS). Institut de Química Computacional i Catàlisi (IQCC) and Departament de Química, Universitat de Girona. Campus Montilivi; E17071 Girona, Catalonia (Spain) miquel.costas@udg.edu,

b) Department of Organic Chemistry, Faculty of Science, Charles University in Prague, Hlavova 2030/8, 12843 Prague 2 (Czech Republic). jana.roithova@natur.cuni.cz

c) Max Planck Institut für Chemische Energiekonversion, Stiftstraße 34 – 36, 45470 Mülheim an der Ruhr (Germany). eckhard.bill@cec.mpg.de

d) Institute of Chemical Research of Catalonia (ICIQ), the Barcelona Institute of Science and Technology, Avinguda Paisos Catalans 16, 43007, Tarragona (Catalonia, Spain). jlloret@iciq.es

e) Catalan Institution for Research and Advanced Studies (ICREA), Passeig Lluïs Companys, 23, 08010, Barcelona (Spain).

TABLE OF CONTENTS

1. Synthesis of complexes 3
2. General procedures 5
3. FT – IR and Raman Spectroscopy of 1 and 4 7
4. Magnetic measurements of 1 7
5. UV – vis spectra of 1 8
6. High – Resolution Mass – Spectrometry of 1 9
7. Photolysis of 1 in solution 11
8. Magnetic field dependent Mössbauer spectrum of 2 in frozen acetone 12
9. Mössbauer measurements of 2 in solid samples 12
10. Magnetic measurements of 2 13
11. XANES Analysis 14
12. Decomposition of 2 16
13. Gas phase reactivity of 2 17
14. XYZ files of geometry optimized structures 19
References: 21

1. Synthesis of complexes

$[Fe^{III}(N_3)(MePy_2tacn)](PF_6)_2$ (1): 108 mg (0.33 mmol) of $MePy_2tacn$ was dissolved with minimum THF. To this solution was added, under vigorous stirring, 150 mg of $Fe^{III}(OTf)_3$ (OTf = CF_3SO_3) (0.32 mmol) suspended in minimum THF; the solution rapidly turned reddish and a dark oil precipitated. The stirring continued for 2 hours. The solution was then decanted and the oil was dried forming a solid. 1 ml of degassed water was added followed by 210 mg (3.2 mmol) of solid NaN_3. The solution readily turned reddish and was stirred, preserved from light, for 2 hours. Then, 1 ml of saturated NH_4PF_6 solved in degassed water was added and a purple solid precipitated. The mixture was stirred for 2 h protected from light. The precipitate was filtered and dried to afford 116 mg of a solid (0.16 mmol, 56 % of yield). The residue was dissolved in acetone, filtered through Celite and recrystallized by slow diethyl ether diffusion at low temperature to provide dark purple crystals.

The same procedure was followed using $Na(^{15}NN_2)$ to obtain $[Fe^{III}(^{15}NN_2)(MePy_2tacn)](PF_6)_2$.

Elemental Analysis (calculated $C_{19}H_{27}N_5FeN_3(PF_6)_2$): C, 32.41; N, 15.34; H, 3.72 (C, 32.0; N, 15.71; H, 3.82).

ESI-MS (m/z experimental (calculated)): $[M-(PF_6)]^+$ = 197.5817 (197.5818), $[M-(N_3)-(PF_6)]^+$ = 190.5803 (190.5803), $[M-(N_2)-(PF_6)]^{2+}$ = 211.5849 (211.5849). FT-IR (Fe – N – N): 2019 cm^{-1}. FT-IR (Fe – **^{15}N = N** / Fe – **N = N** = N): 1998 / 2021 cm^{-1}.

$[Fe^{II}(N_3)(MePy_2tacn)]OTf$ (4): 50 mg (0.074 mmol) of $[Fe^{II}(OTf)(MePy_2tacn)](OTf)$ and 48 mg (0.74 mmol) of NaN_3 were dissolved in MeOH (3 mL) under a N_2 atmosphere, and the resulting solution was stirred overnight protected from light. The resulting orange solution was dried and the obtained orange solid was dissolved in the minimum CH_2Cl_2, filtered through Celite and the complex crystallized protected from light by slow diethyl ether diffusion to provide 32 mg (0.055 mmol, 75% of yield) of highly hygroscopic orange needles.

Elemental Analysis (calculated $C_{19}H_{27}N_5FeN_3CF_3SO_3 \cdot 1/2H_2O$): C, 41.91; N, 18.81; H, 4.36 (C, 41.32; N, 19.27; H, 4.85).

ESI-MS (m/z experimental (calculated)): $[M-(N_3)]^+$=530.1 (530.1), $[M-(SO_3CF_3)]^+$=423.1, $[M-(N_3)(SO_3CF_3)]^{2+}$=190.5 (190.6). IR (Fe – N – N): 2055 cm^{-1}

$[Fe^{II}(MePy_2tacn)(MeCN)](CF_3SO_3)_2$ 3, was prepared as previously described.[1]

Synthesis of ^{57}Fe enriched samples.

$[^{57}Fe^{II}(N_3)(MePy_2tacn)]OTf$, **^{57}Fe-(4)**, was prepared as (**4**), starting with $^{57}Fe(CF_3SO_3)_2 \cdot 2CH_3CN$.

$[^{57}Fe^{III}(N_3)(MePy2tacn)](PF_6)_2$, **^{57}Fe-(1)** was prepared using **^{57}Fe-(4)** as starting material: In a glass vial, protected from light by an aluminum foil, and under a N_2 atmosphere, 5 mg of **^{57}Fe-(4)** were solved in 1.5 ml of dichloromethane. Then 2.24 mg of Ag(OTf) (1.2 eq) were added as a solid and the mixture was stirred for 20h. The solution was filtered with an Acrodisk® filter and solvent was removed under vacuum to obtain a reddish oil. The vial containing the reddish oil was again protected from light, and 2.9 mg (5 eq) of NaN_3 and 0.4 ml of water were

added. The resulting mixture was stirred for 2 h and then 0.15 ml of a saturated solution of $(NH_4)PF_6$ in water were added, causing the immediate formation of a precipitate. The mixture was stirred for 2h. The supernatant was separated by decantation, and the purple precipitate was washed with water and dichloromethane. The solid was dried under vacuum and recrystallised protected from light in acetone with slow diffusion of diethyl ether, providing 4.4 mg of dark purple crystals of the compound (70%), which purity was confirmed by UV-vis spectroscopy.

2. General procedures

Photolysis experiments.

Photolysis of solid powder samples. Solid powder samples (*ca.* 50 mg) of **1** were suspended in an open liquid nitrogen bath and photolysed under strong stirring at 77 K, using a 470 or a 530 nm LED lamp. After 5 h of illumination, product sample (**2**) was kept at 77 K and transferred to the appropriate holder for Mössbauer, EPR and SQUID measurements.

Photolysis of frozen solution samples for EPR and Mossbauer spectroscopy. Acetone solutions of **1** (2 mM) were prepared in an anaerobic box, in a vial protected from light. EPR tubes were filled with 0.1 ml of this solution and the tubes capped with a rubber septum. Samples were frozen with liquid N_2, and the tubes vacuum pumped. While maintaining samples frozen, the EPR tubes were flame-sealed while keeping the vacuum on them. In the case of Mössbauer samples, the solution was poured into a Mossbauer holder under air, and frozen immediately in a liquid nitrogen bath, trying to keep contact with air as minimum as possible. All the frozen samples were irradiated for 6h in a liquid nitrogen bath with a 530 nm LED, both for EPR and Mössbauer samples. In the case of the EPR tubes, the samples were moved every 20 or 30 minutes to allow a more homogeneous irradiation.

Mössbauer Spectroscopy. Mössbauer spectra were recorded on a conventional spectrometer with alternating constant acceleration of the γ – source (^{57}Co/Rh, 1.8 GBq), which was kept at room temperature. The minimum experimental line width was 0.24 mm/s (full width at half – height). The sample temperature was maintained constant in an Oxford Instruments Variox cryostat. Isomer shifts are quoted relative to iron metal at 300 K.

EPR Spectroscopy. X – band EPR derivative spectra were recorded on a Bruker ELEXSYS E500 spectrometer equipped with the Bruker dual – mode cavity (ER4116DM) and a helium flow cryostat (Oxford Instruments ESR 900). Microwave frequencies were calibrated with a Hewlett – Packard frequency counter (HP5352B), and the field control was calibrated with a Bruker NMR field probe (ER035M). The powder spectra were simulated with the program esimX_gfit (by E.B.) using effective g values and anisotropic line widths (Lorentzian line shapes were used).

XAS data collection and processing: Samples for X – ray absorption measurements were prepared as 4 mM solutions in acetone loaded in sample holders and stored at liquid nitrogen temperatures until spectra adquisition. Compound **2** was generated by loading a solution of **1** in a sample holder and photolysing the sample in a liquid nitrogen bath using a 570 nm (green) light for 5 hours. XAS data on compounds **1** and **2** was collected at the SOLEIL synchrotron, SAMBA beamline, under anaerobic conditions at 25 K using a liquid helium cryostat. The SAMBA beamline is also equipped with a Si (220) double crystal monochromator and a Canberra 35 – element Ge detector. Compound **4**, on the other hand was run at 80 K using a liquid helium cryostat from the DIAMOND beamline B18 equipped with a Si (111) double crystal monochromator and an 8 – element Ge detector.

Data processing was carried out with the Athena software package.[2] A linear pre – edge followed by a quadratic post – edge function were used for baseline subtraction and normalization of the edge jump to 1.

Energy calibration was performed using the first inflection point of Fe foil taken as 7111.2 eV. EXAFS were extracted using the AUTOBK algorithm with E0 taken as the first inflection point of the rising edge, having an R_{bkg} of 1 and a spline with a k – range of 1 to 15 $Å^{-1}$. EXAFS analysis was carried out with Artemis, employing the Iffefit engine and FEFF6 code.[3,4] The k^3 – weighted data was fit in R – space between 1 and 3 Å, having a k – range of 2 – 14 Å, and a Hannings window with a dk of 2. Fits were carried out with a global S_0^2 of 0.9 as well as a global ΔE0. Scattering paths were fit in terms of ΔR_{eff} and $\Delta \sigma^2$, and the goodness of fit was the R_{fator} (%R) and reduced χ^2 (χ^2_v) were minimized as previously described.[5,6]

Theoretical calculations: Theoretical calculations were carried out with the ORCA software package.[7] Geometry optimizations were carried out using a TPSS functional with a def2 – TZVP as well as a def2 – TZVP/J auxiliary basis set on all atoms.[8,9] Subsequent single point calculations to explore the electronic structure and calculate the XAS spectra employed the TPSSh functional with an expanded CP(PPP) basis set[10] on the iron and a def2 – TZVP basis set on the remaining atoms. The above calculations employed a dense integration grid (ORCA Grid 5 = Lebedev 434 points) along with the Grimme and coworkers DFT – D3BJ dispersion correction.[11,12]. In addition solvent effects were included using a conductor like screening model (COSMO) using acetone as solvent.[13] XAS spectra was calculated using the TD – DFT method employing the Tamm – Dancoff approximation.[14,15]

Gas phase reactivity: Reactivity measurements were carried out using a TSQ 7000 mass spectrometer with quadrupole – octopole – quadrupole configuration equipped with an electrospray ion source. The first quadrupole selects the ion of interest, the octopole filled with a gas serves as a reaction/collision cell and the third quadrupole analyzes the products of the collisions. Ions were generated from 100 µM solution of $[Fe^{III}(N_3)(MePy_2tacn)](PF_6)_2$ (**1**) in acetone. Spraying conditions: 3.5 kV spray voltage, 60 psi sheath gas pressure, 0 V capillary voltage, 70 V tube lens voltage, 200 µl/hour flow rate. Reaction rates were compared relatively at 0.1 mTorr pressure and nominally zero collision energy that was determined from retarding potential analysis. Typical full – width at half maximum of the kinetic energy distribution of the ions was 0.8 eV.

3. FT – IR and Raman Spectroscopy of 1 and 4

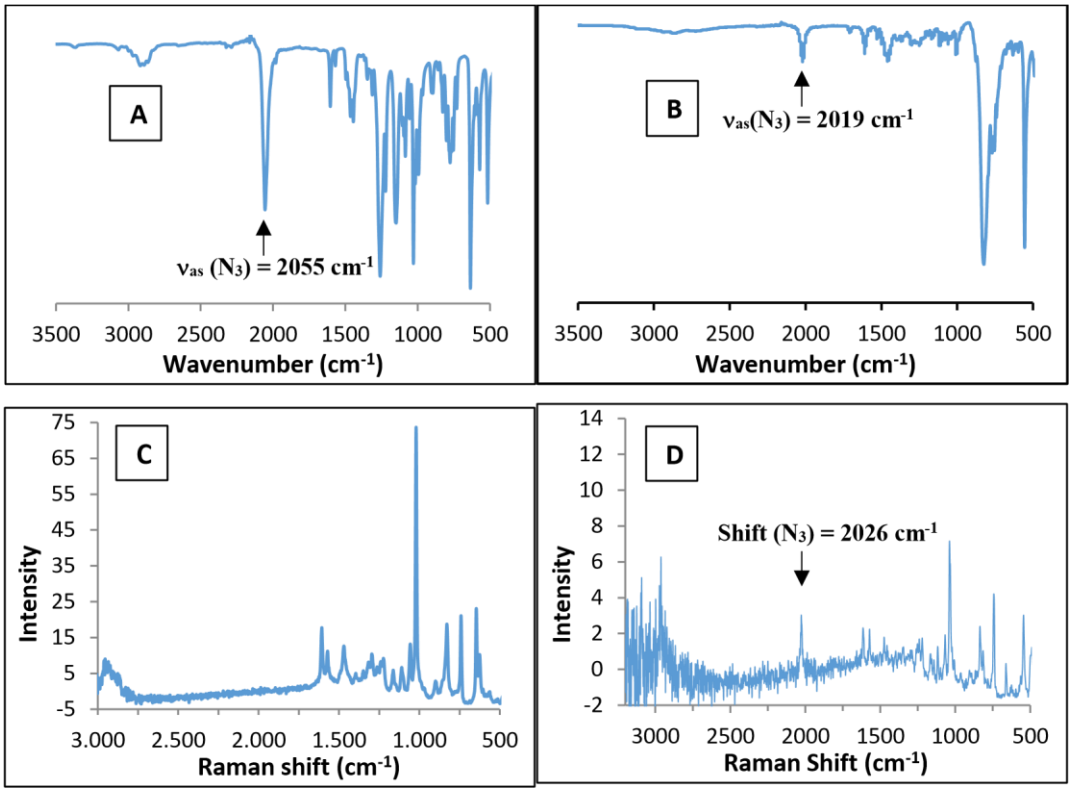

Figure S1. (A) FT – IR spectra of iron (II) azide **4** and (B) iron (III) azide **1**. (C) Raman spectra of **4** and (D) **1**; ≈ 2000 cm^{-1} features are typical for asymmetric stretching of Fe – N_3.[16]

4. Magnetic measurements of 1

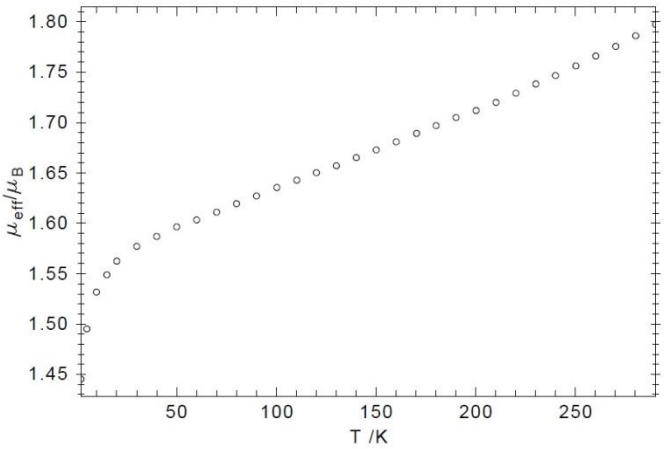

Figure S2. Temperature dependence of the effective magnetic moment for complex **1**.

5. UV – vis spectra of 1

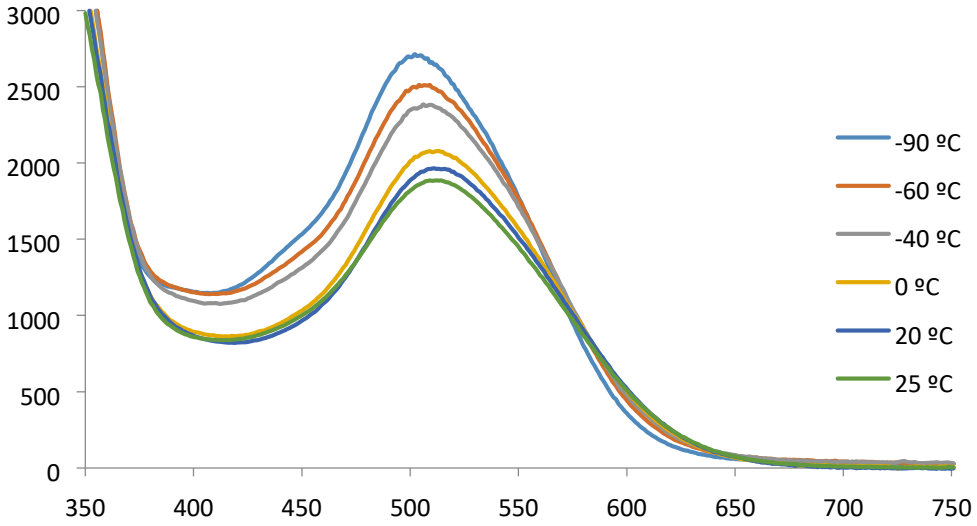

Figure S3. UV – Vis spectra for complex **1** in acetone at different temperatures.

6. High – Resolution Mass – Spectrometry of 1

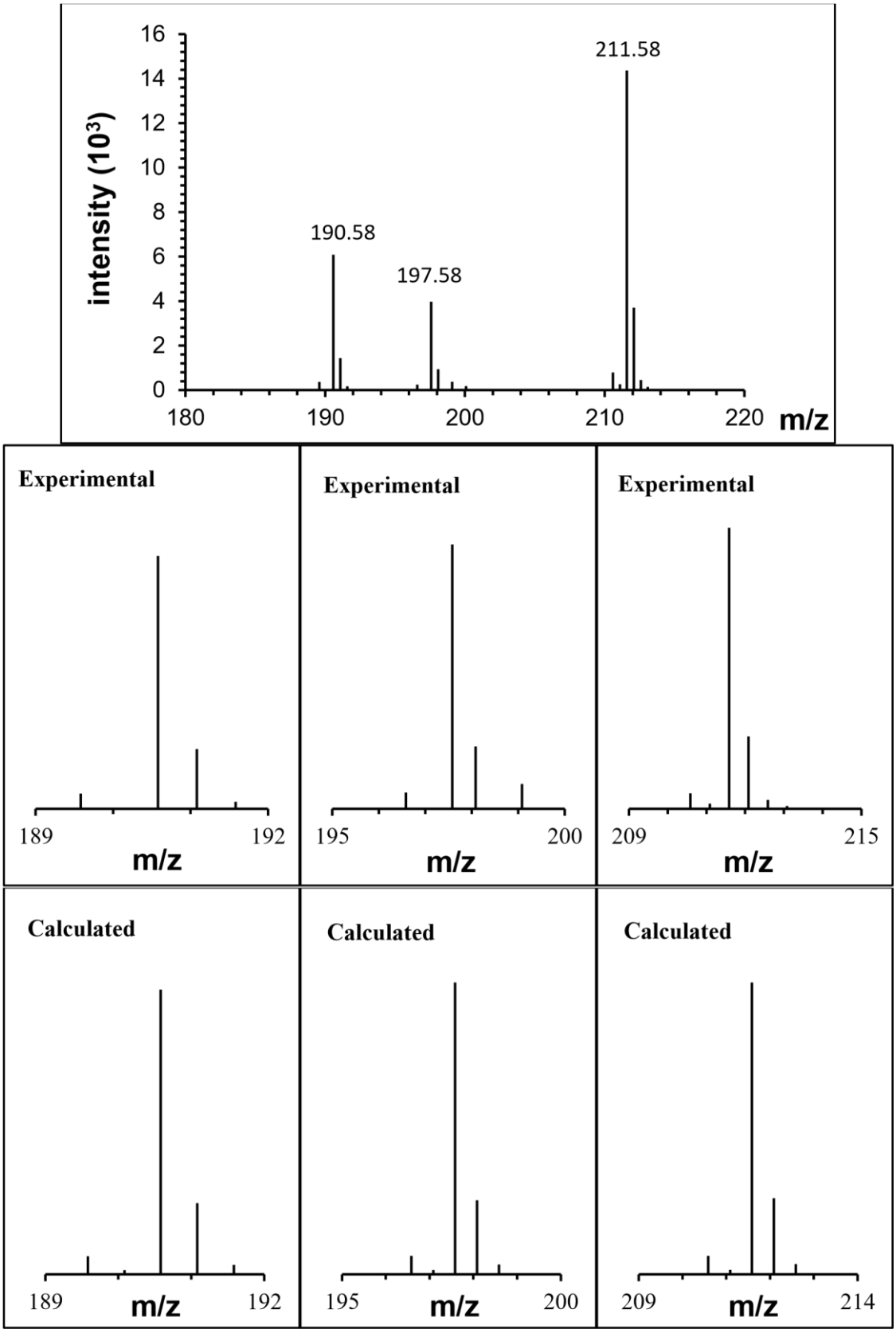

Figure S4. High resolution mass spectra of **1** in acetone, insets are ions for $Fe^{II}(L)$, $Fe^{III}(N_3)(L)$ and $Fe^{V}(N)(L)$, with simulated peaks (L = $MePy_2tacn$).

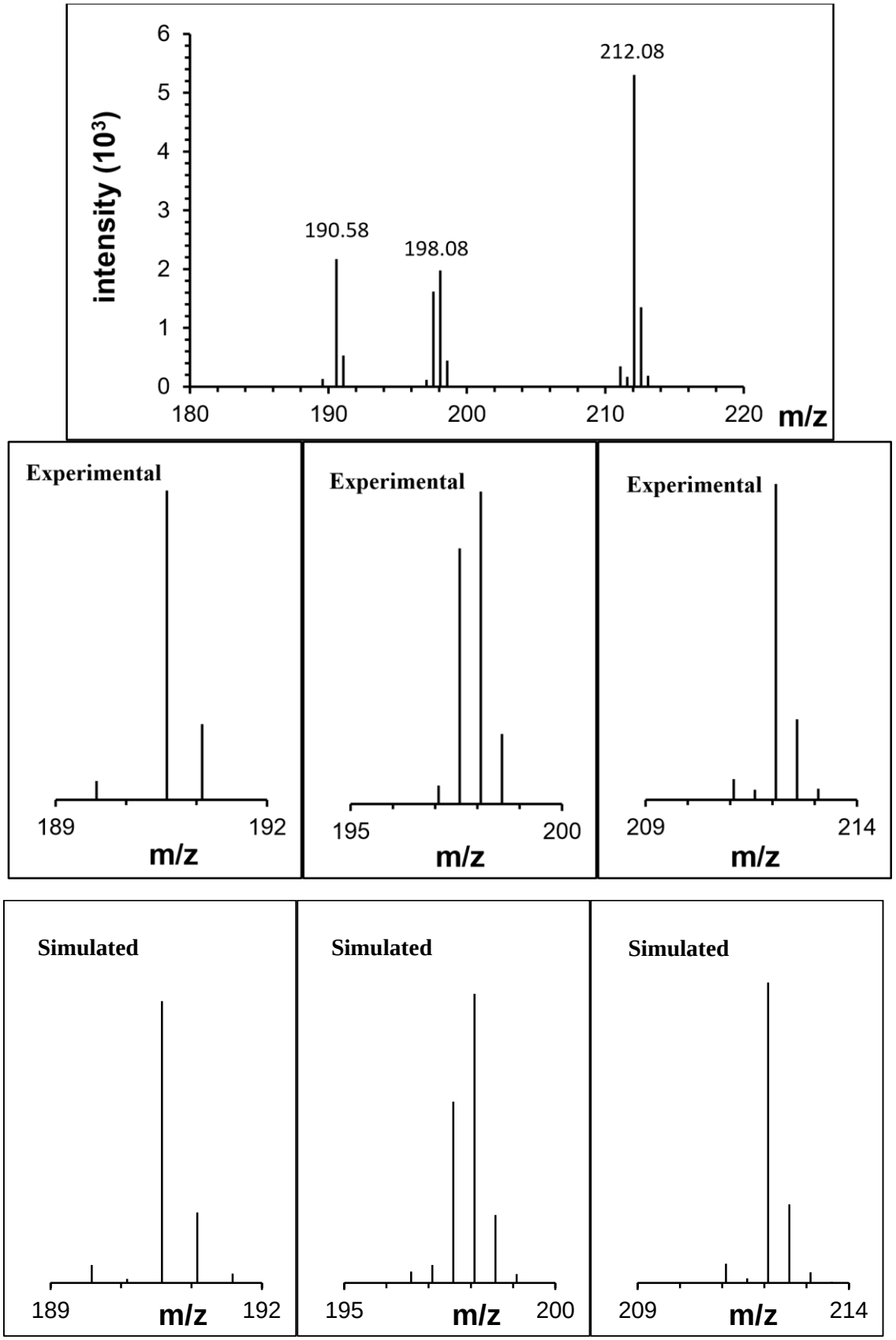

Figure S5. High resolution mass spectra of **1** – $^{15}N_3$ in acetone, below simulated ions of $[Fe^{II}(L)]^{2+}$, $[Fe^{III}(^{14/15}N_3)(L)]^{2+}$and $[(Fe^{V}(N)(L)]^{2+}$ / $[Fe^{V}(^{15}N)(L)]^{2+}$species. L = $MePy_2tacn$.

7. Photolysis of 1 in solution

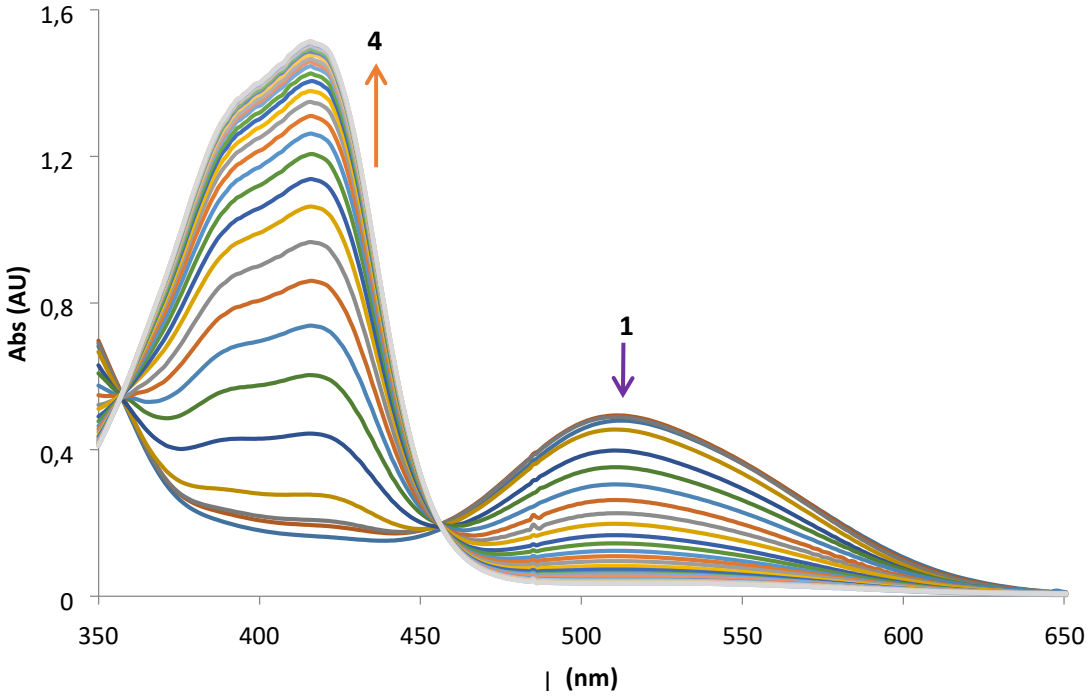

Figure S6. Photolysis of complex **1** with 470 nm LED (0.2 mM acetonitrile at 233 K).

8. Magnetic field dependent Mössbauer spectrum of 2 in frozen acetone

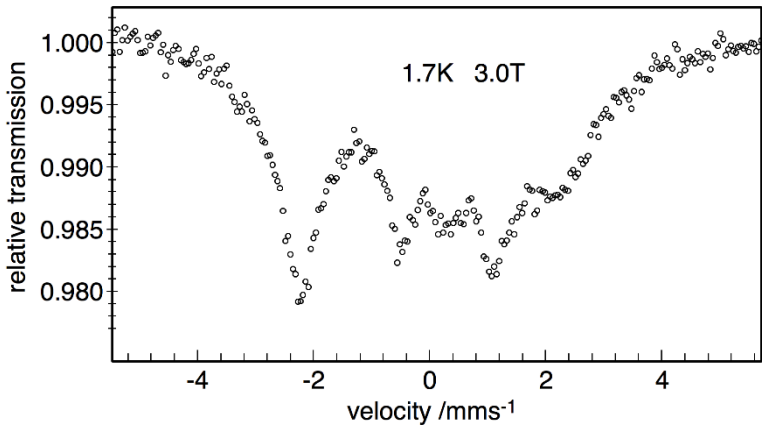

Figure S7. Magnetic Mössbauer spectrum of the photoproduct recorded after photolysis of 57-Fe-enriched compound **1** recorded at 1.7 K in order to slow down spin relaxation, and with a field of 3 T applied perpendicular to the gamma ray.

9. Mössbauer measurements of 2 in solid samples

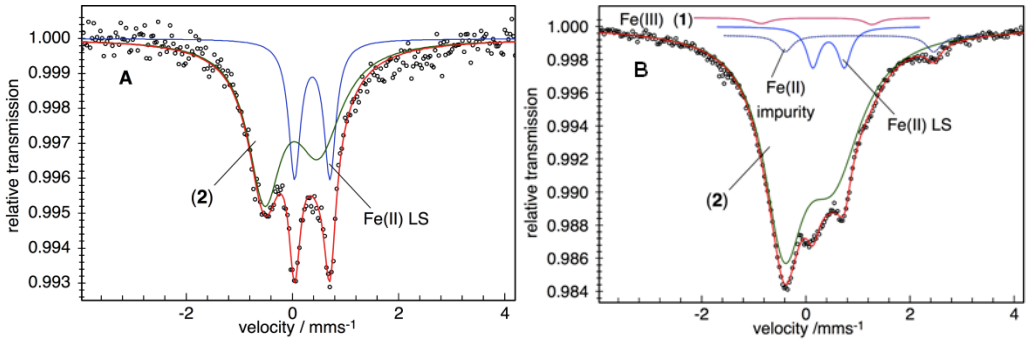

Figure S8. (**A**) Zero-field Mössbauer spectrum of solid complex **1** after 4.5 h photolysis at 77 K with a 470 nm (blue) LED. The green and blue lines in (A) are Lorentzian doublets accounting for a new low-spin iron(II) species (Fe(II) LS) and the high-valent photo-product (**2**); the red is the superposition of the subspectra. The extended asymmetry of the subspectrum from **2** presumably results from intermediate spin relaxation. (**B**) Zero-field Mössbauer spectrum of solid complex **1** after 5 h photolysis at 77 K with a 530 nm (green) LED. The Mössbauer spectrum (B) was fitted with four Lorentzian doublets accounting for i.) Iron(III) starting material (**1**, 1%, in pink), ii.) ferrous impurity, iron(II) HS (3%, in dark blue), and the photoproducts iii.) Iron(II) LS (6%, in blue), and iv.) the high-valent photo-product (**2**, 89%, in green).

10. Magnetic measurements of 2

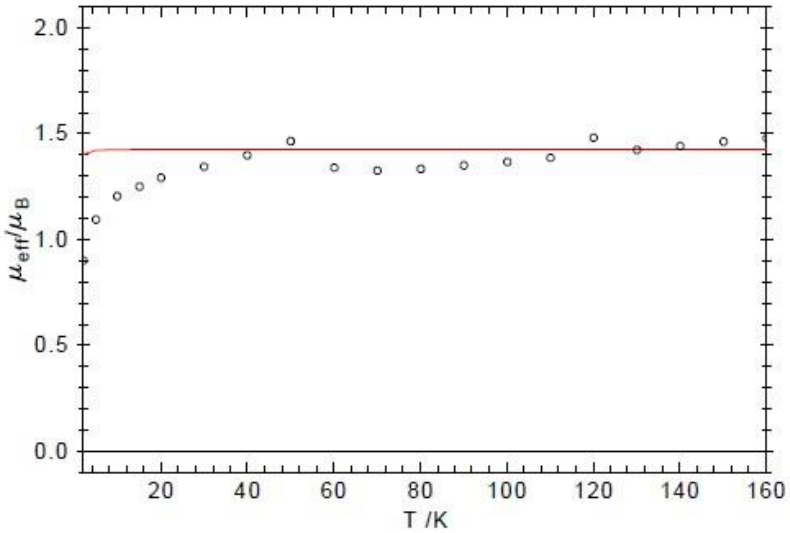

Figure S9. SQUID measurement of solid complex **2** after photolysis at 77 K with a 470 nm LED in a beaker. Red line is the simulation of a mixture of 75 % of an S = ½ and a 25 % of S = 2 species.

11. XANES Analysis

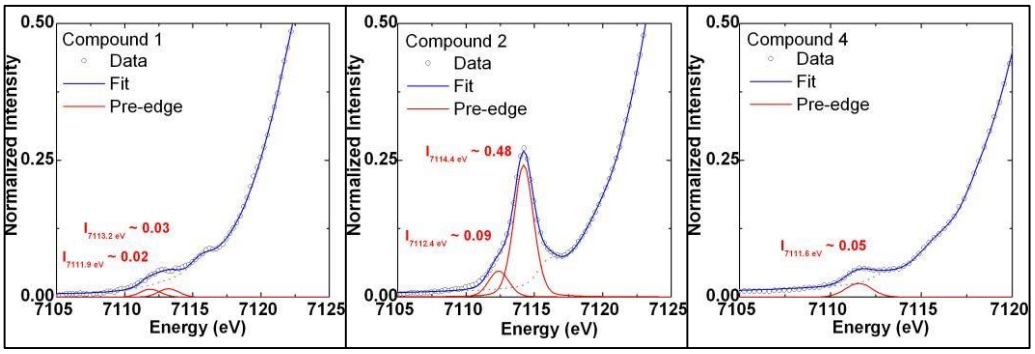

Figure S10. Fe K pre – edge XANES region for compounds **1**, **2** and **4** highlighting the 1s → 3d feature fit with a cumulative Gaussian lorentzian sum function having 0.75% Gaussian character.

Table S1 Selected EXAFS fits for **2**. Fits carried out in r – space (Δk = 2 – 14 Å^{-1}; Δr = 1 – 3 Å) with a Hanning window (dk 2), a *k* – weight = 3 and S_0 = 0.9. Bond distances and disorder parameters (Δr_{eff} and σ^2) were allowed to float having initial values of 0.0 Å and 0.003 Å^2 respectively, with a universal E_0 initially set to first inflection point of the rising edge and ΔE_0 = 0 eV. (Fits highlighted in blue are the best models; values highlighted in red are either statistically or physically erroneous; σ^2 reported as x10^3 Å^2).

							Fe-N/O*			Fe-N/O*			Fe-N/O*		
FIT	Δk	Δr	*Var.*	R_{FACTOR}	χ^2_v	ΔE_0	N	r(Å)	σ^2	N	r(Å)	σ^2	N	r(Å)	σ^2
1	2.0-14.0	1.0-3.0	8	0.044	12.5	2.38	1	1.64(1)	2(2)	3	1.98(1)	2(1)	2	2.05(4)	9(6)
2	2.0-14.0	1.0-3.0	6	0.137	30.0	-1.97	-	-	-	4	1.99(2)	3(2)	2	2.03(6)	9(9)
3	2.0-14.0	1.0-3.0	6	0.068	15.0	-0.73	1	1.65(2)	2(2)	-	-	-	5	1.99(1)	5(1)
4	2.0-14.0	1.0-3.0	8	0.036	10.2	3.81	1	1.64(1)	2(1)	2	1.98(1)	0(1)	2	2.05(2)	5(2)
5	2.0-14.0	1.0-3.0	8	0.029	8.1	2.57	1	1.64(1)	3(1)	3	1.98(1)	2(1)	2	2.05(2)	7(3)

	Fe--C			Fe--C			Fe--C-N--Fe			Fe--C-N--Fe		
FIT	N	r(Å)	σ^2	N	r(Å)	σ^2	N	r(Å)	σ^2	N	r(Å)	σ^2
1	8	2.86(4)	9(6)	5	2.96(8)	9(6)	-	-	-	-	-	-
2	8	2.84(6)	9(9)	5	2.95(12)	9(9)	4	3.05(12)	9(9)	4	3.12(12)	9(9)
3	8	2.79(1)	5(1)	5	2.94(3)	5(1)	4	3.05(3)	5(1)	4	3.12(3)	5(1)
4	8	2.86(2)	5(2)	6	3.00(4)	5(2)	4	3.10(4)	5(2)	4	3.17(4)	5(2)
5	8	2.86(2)	7(3)	5	2.99(3)	7(3)	4	3.08(3)	7(3)	4	3.16(3)	7(3)

*Although EXAFS can not differentiate between O/N/C scattering paths, chemical intuition was used for description to facilitate comparison with theoretically derived structure

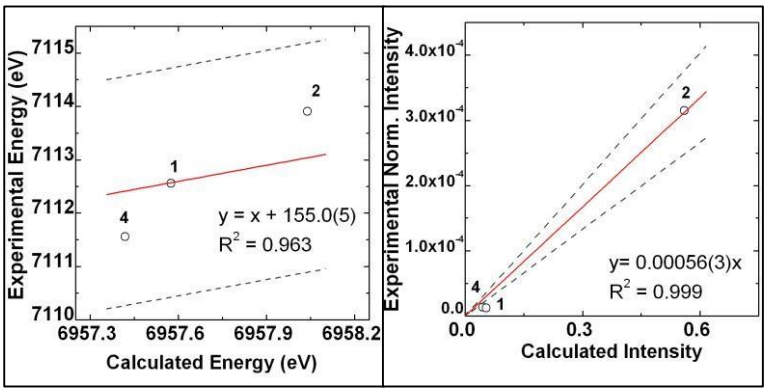

Figure S11. Correlation between calculated and experimental Fe K pre – edge intensity averaged energies (left) and total intensities (right) for **1**, **2** and **4**.

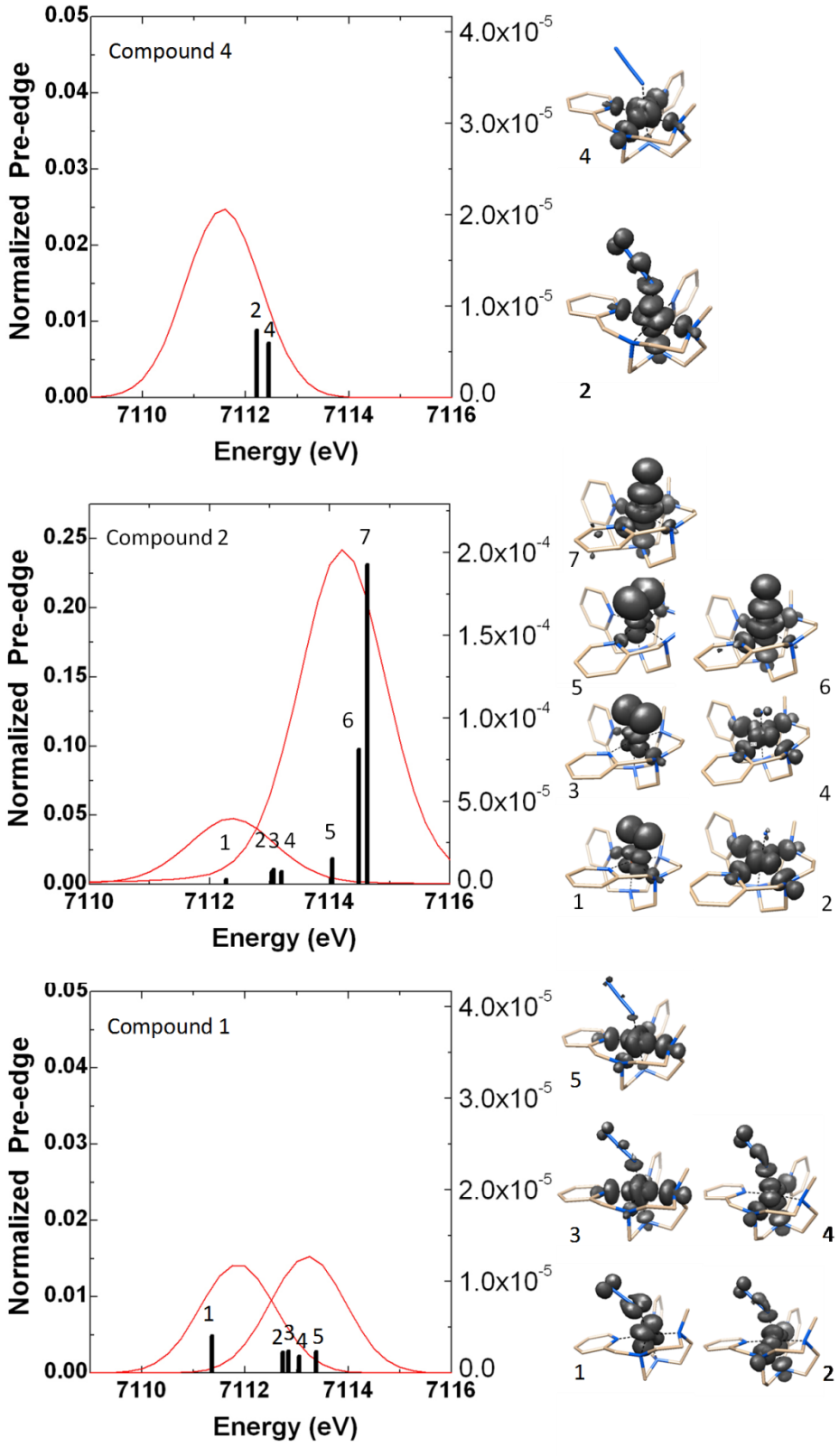

Figure S12. Correlation between experimental Fe K pre – edges and calculated transitions including the difference density maps for: **1**, **2** and **4**. Transitions were shifted by 155.0 eV to match experiment.

12. Decomposition of 2

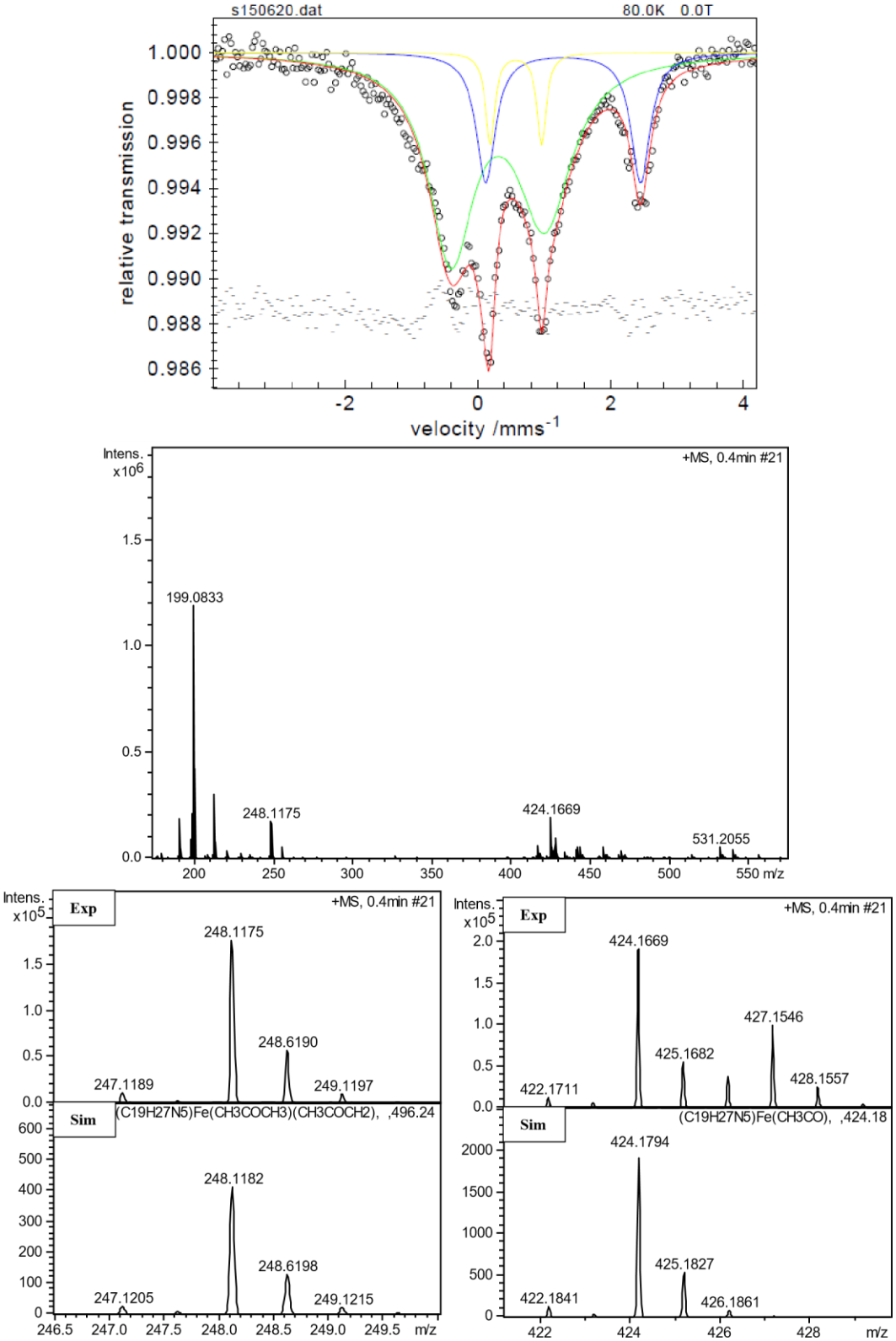

Figure S13. (Top) Mössbauer spectra after decomposition of solid **2** at room temperature under anaerobic conditions. (Below) HR – MS analysis of melted sample after photolysis of **1** to **2** during online mass spectrometry studies; insets show the experimental and simulated ions 248.12 and 424.17, tentatively assigned to species $[Fe^{II}(COCH_3)(MePy_2tacn)]^+$ and $[Fe^{III}(COCH_3)(CH_3COCH_3)(MePy_2tacn)]^{2+}$ suggesting that **2** could be reacting with acetone.

13. Gas phase reactivity of 2

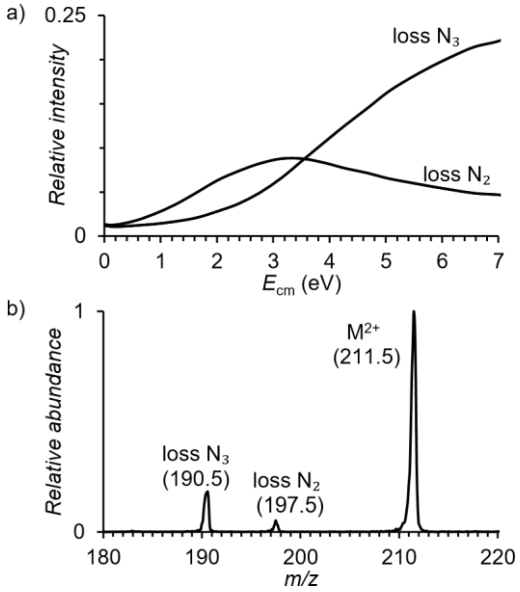

Figure S14. (a) Dependence of the relative cross section of the loss of N_2 and N_3 from $[Fe^{III}(N_3)(MePy_2tacn)]^{2+}$ on the collision energy. Collision gas was xenon (p = 0.1 mTorr). Total intensity is normalized to 1 at each energy. (b) CID spectrum of mass – selected $[Fe^{III}(N_3)(MePy_2tacn)]^{2+}$ at E_{cm} = 18.3 eV.

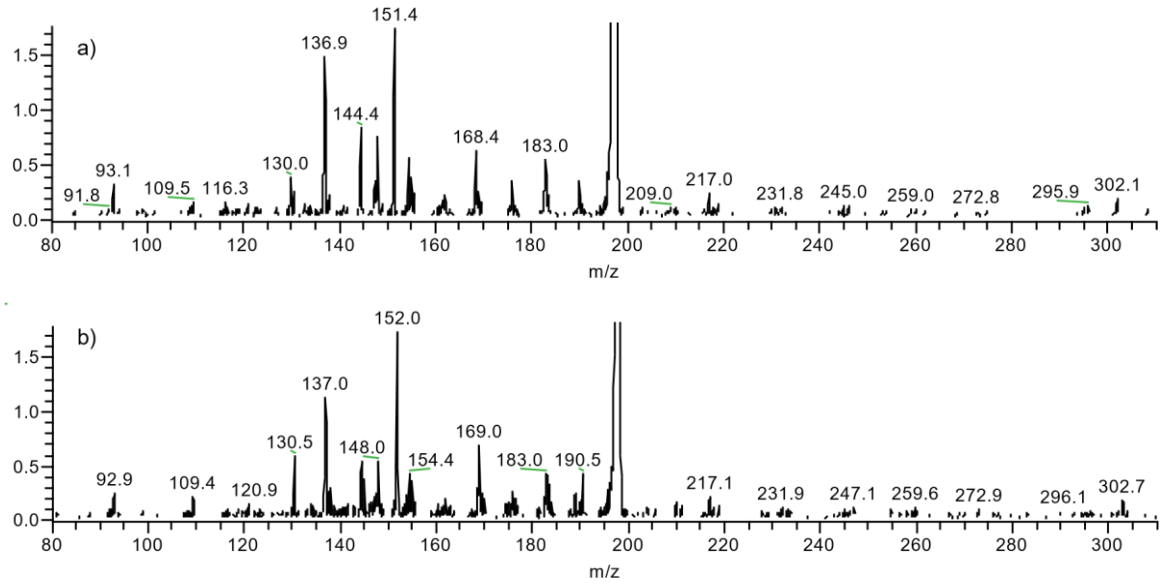

Figure S15. Collision induced dissociation (CID) spectrum of (a) $[Fe^{V}(^{14}N)(MePy_2tacn)]^{2+}$ and (b) $[Fe^{V}(^{15}N)(MePy_2tacn)]^{2+}$ with 0.1 mTorr of Xenon at 5 eV collision energy (center of mass).

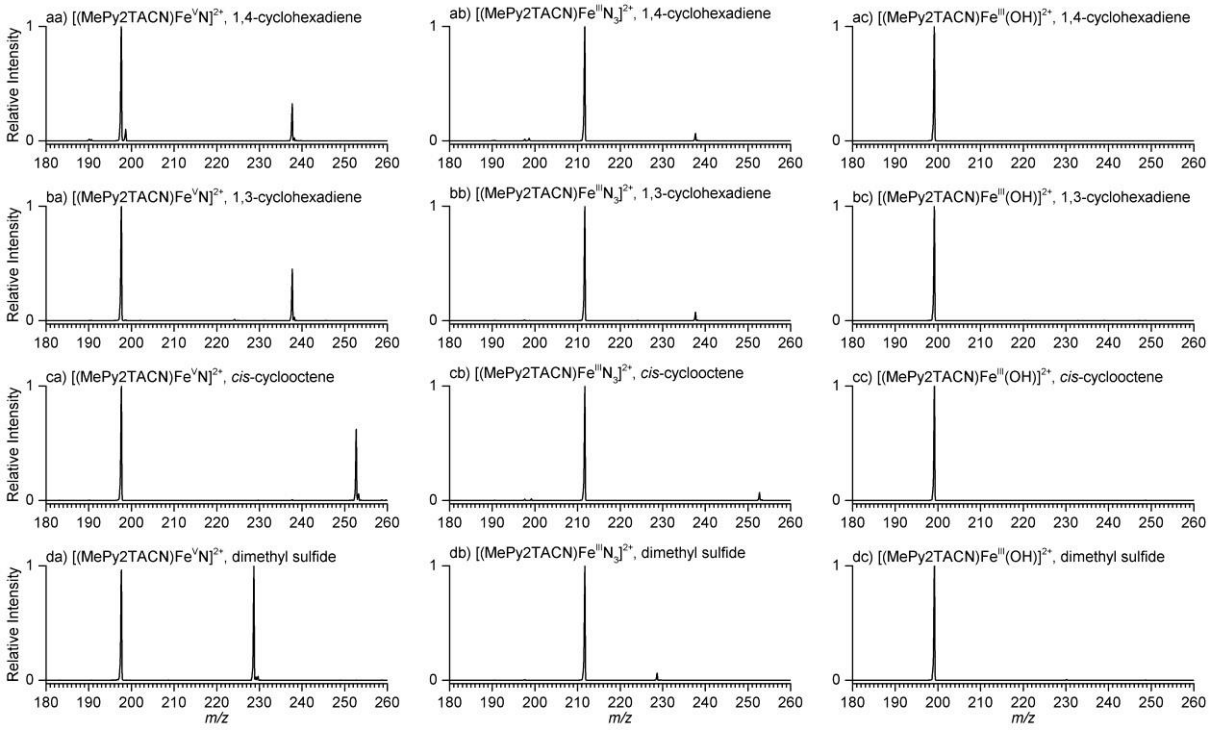

Figure S16. Reactions of (xa) $[Fe^{V}(N)(MePy_2tacn)]^{2+}$ (*m/z* = 197.5), (xb) $[Fe^{III}(N_3)(MePy_2tacn)]^{2+}$ (m/z = 211.5) and (Xc) $[Fe^{III}(OH)(MePy_2tacn)]^{2+}$ dications with ~ 0.1 mTorr of (aX) 1, 4 – cyclohexadiene, (bX) 1, 3 – cyclohexadiene, (cX) *cis* – cyclooctene and (dX) dimethyl sulfide in the collision cell at nominally zero collision energy. Collisions of $[Fe^{III}(N_3)(MePy_2tacn)]^{2+}$ with the reagent gas are accompanied by partial fragmentation to the nitride , which explains the small observed reactivity analogous to that of the nitride.

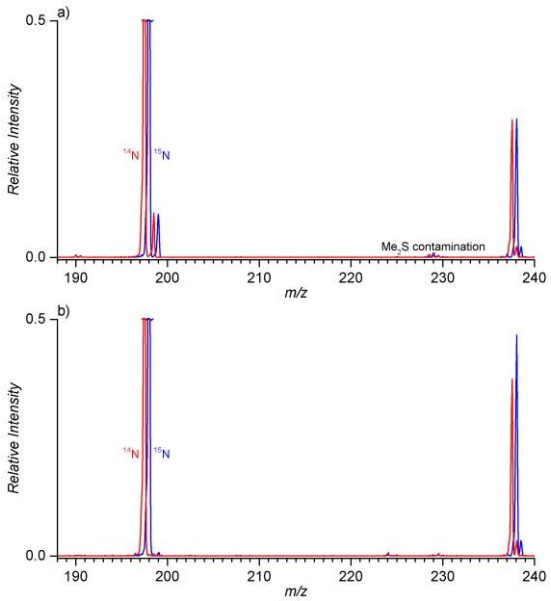

Figure S17. Reactions of $[Fe^{V}(^{15}N)(MePy_2tacn)]^{2+}$ (*m/z* = 198) with (a) 1, 4 – cyclohexadiene, (b) 1, 3 – cyclohexadiene (0.1 mTorr) at nominally zero collision energy.

14. XYZ files of geometry optimized structures

Compound 1 S=1/2 E = -2442.591 Eh

Fe	1.976183	0.378658	13.560691
N	3.227752	-1.153380	13.514145
C	4.574691	-1.140139	13.601595
H	5.046105	-0.171563	13.710756
N	0.602760	-1.030675	13.851832
C	5.329048	-2.302713	13.547767
H	6.408395	-2.239406	13.623153
N	2.018942	0.556186	15.569612
C	4.677928	-3.526267	13.401523
H	5.241576	-4.452442	13.367399
N	0.439146	1.712738	13.639829
C	3.289093	-3.543030	13.295499
H	2.745640	-4.473497	13.172768
N	3.409850	1.717370	13.660981
C	2.590195	-2.343895	13.342675
N	1.824117	0.298066	11.670091
C	1.105476	-2.245558	13.143950
H	0.586033	-3.144100	13.487628
H	0.893916	-2.109953	12.078674
C	0.438719	-1.292095	15.335021
H	0.283259	-2.360173	15.501360
H	-0.463718	-0.776644	15.662655
N	2.690360	-0.117413	10.922143
N	3.454886	-0.495443	10.147256
C	1.655280	-0.798464	16.099724
H	1.446275	-0.746913	17.172794
H	2.514616	-1.451473	15.946624
C	1.021606	1.598127	16.021748
H	0.135159	1.074668	16.380356
H	1.435005	2.155427	16.865075
C	0.678050	2.525523	14.874022
H	-0.208488	3.122526	15.114460
H	1.499708	3.209275	14.654227
C	0.347108	2.636428	12.471989
H	-0.455064	3.359940	12.651433
H	0.139728	2.057718	11.573833
H	1.293946	3.164436	12.357129
C	-0.852062	0.926623	13.756419
H	-1.159988	0.925437	14.802792
H	-1.637427	1.431630	13.189472
C	-0.653708	-0.486852	13.242416
H	-1.510817	-1.120376	13.493167
H	-0.503688	-0.492255	12.161808
C	3.413129	0.944055	15.938097
H	4.020683	0.033305	15.937861
H	3.450416	1.369411	16.944366
C	3.936768	1.894103	14.903254
C	4.916126	2.846157	15.148976
H	5.304423	2.965940	16.154486
C	5.382682	3.629950	14.095010
H	6.147942	4.379335	14.266307
C	4.847026	3.438613	12.822906
H	5.178631	4.025101	11.973883
C	3.859739	2.480832	12.641435
H	3.404390	2.309108	11.674389

Compound 2 S=1/2 E = - -2332.981 Eh

Fe	1.976242	0.373452	13.451529
N	3.224483	-1.173234	13.461304
C	4.567241	-1.157360	13.560306
H	5.039887	-0.186720	13.643585
N	0.615134	-1.024975	13.828059
C	5.317102	-2.325571	13.549899
H	6.395955	-2.265649	13.634870
N	2.024859	0.546570	15.599464
C	4.661131	-3.549218	13.433186
H	5.220969	-4.478426	13.431716
N	0.437074	1.728520	13.634655
C	3.272627	-3.564694	13.315287
H	2.726388	-4.496321	13.216610
N	3.389705	1.723271	13.642836
C	2.581121	-2.360702	13.320402
N	1.881237	0.346116	11.852566
C	1.100700	-2.245952	13.113305
H	0.563859	-3.135350	13.453265
H	0.900521	-2.097220	12.047011
C	0.461442	-1.296178	15.314116
H	0.303845	-2.366467	15.463262
H	-0.442208	-0.784449	15.644383
C	1.672284	-0.810320	16.095532
H	1.447691	-0.805112	17.168051
H	2.534532	-1.457840	15.931320
C	1.026419	1.578610	16.031317
H	0.133827	1.058771	16.381567
H	1.418174	2.148148	16.878742
C	0.687499	2.514521	14.883255
H	-0.195537	3.114725	15.129914
H	1.511171	3.197845	14.670278
C	0.331934	2.671521	12.485469
H	-0.482386	3.379303	12.673228
H	0.138790	2.102802	11.576680
H	1.271111	3.215591	12.382023
C	-0.849152	0.933369	13.752072
H	-1.154585	0.930349	14.799102
H	-1.638148	1.434690	13.187055
C	-0.655147	-0.481911	13.239825
H	-1.505326	-1.115532	13.512708
H	-0.528269	-0.494546	12.155604
C	3.408666	0.952676	15.937330
H	4.034755	0.053638	15.936162
H	3.471481	1.396521	16.935826
C	3.913069	1.899954	14.885567
C	4.889404	2.858618	15.125409
H	5.274994	2.982234	16.131530
C	5.355947	3.640706	14.071680
H	6.117412	4.394013	14.243013
C	4.828985	3.439094	12.797067
H	5.164979	4.019175	11.945320
C	3.847743	2.477125	12.616456
H	3.403849	2.280967	11.647849

Compound 2 S=3/2 E = -2332.943 Eh

Fe	1.983198	0.391195	13.536031
N	3.200559	-1.178944	13.477052
C	4.545340	-1.159475	13.576302
H	5.016988	-0.191358	13.682442
N	0.616677	-1.026537	13.830579
C	5.296875	-2.325236	13.538799
H	6.375372	-2.261287	13.625155
N	2.020635	0.564968	15.633816
C	4.646664	-3.549067	13.396515
H	5.210055	-4.475720	13.375328
N	0.435569	1.716576	13.660612
C	3.258469	-3.565765	13.278278
H	2.713831	-4.495781	13.158423
N	3.411275	1.721650	13.642432
C	2.561877	-2.365962	13.309075
N	1.916970	0.345590	11.782126
C	1.088291	-2.237029	13.093258
H	0.533924	-3.124561	13.408910
H	0.904173	-2.057274	12.029166
C	0.470678	-1.303994	15.318148
H	0.335967	-2.377458	15.467331
H	-0.443763	-0.813203	15.651081
C	1.672844	-0.801608	16.112457
H	1.435366	-0.808551	17.182121
H	2.543918	-1.438301	15.952968
C	1.009082	1.585629	16.061502
H	0.119303	1.055363	16.403096
H	1.387418	2.159420	16.911873
C	0.672183	2.516388	14.908301
H	-0.218304	3.110849	15.138810
H	1.492987	3.203626	14.695823
C	0.353937	2.636654	12.489533
H	-0.473153	3.336966	12.645780
H	0.193211	2.045100	11.588812
H	1.289863	3.188316	12.402081
C	-0.852105	0.921470	13.770636
H	-1.151125	0.902209	14.818854
H	-1.638353	1.437132	13.215244
C	-0.643399	-0.476448	13.229148
H	-1.493267	-1.126023	13.462296
H	-0.484648	-0.455502	12.149251
C	3.402991	0.991069	15.963335
H	4.036040	0.097012	15.982774
H	3.462764	1.457728	16.951332
C	3.914039	1.921995	14.893736
C	4.886285	2.886201	15.119501
H	5.267814	3.037135	16.123275
C	5.355422	3.645205	14.047662
H	6.112385	4.405320	14.209996
C	4.845168	3.417965	12.769038
H	5.191076	3.984575	11.912438
C	3.872986	2.445650	12.598946
H	3.433130	2.205280	11.637092

Compound 4 S=0 E=-2442.758 Eh

Fe	5.047414	3.398126	1.098482
N	5.986802	3.041049	-0.628195
C	7.118874	4.026934	-0.790940
H	7.184711	4.351439	-1.833472
H	8.050302	3.509905	-0.555307
C	6.927217	5.229812	0.127624
H	7.855953	5.808920	0.197575
H	6.139436	5.885399	-0.245309
N	6.493582	4.732558	1.466618
C	7.640099	4.087097	2.200855
H	8.050598	4.784365	2.936823
H	8.428386	3.882082	1.474850
C	7.180697	2.804939	2.870915
H	8.045968	2.216112	3.201695
H	6.560998	3.018947	3.743892
N	6.337655	2.024118	1.918310
C	7.182201	1.461463	0.798171
H	7.387468	0.403382	0.985157
H	8.144065	1.977840	0.796861
C	6.473739	1.634454	-0.534412
H	7.143342	1.381795	-1.366302
H	5.585651	1.000967	-0.577890
C	4.961947	3.215803	-1.692316
H	4.352453	2.306458	-1.698471
H	5.417252	3.336609	-2.681581
C	4.090538	4.381646	-1.328396
C	3.408982	5.151421	-2.260821
H	3.553488	4.956315	-3.318630
C	2.543833	6.154616	-1.824436
H	2.001145	6.766231	-2.537485
C	2.390124	6.345991	-0.451879
H	1.720743	7.102877	-0.057517
C	3.111727	5.554035	0.429639
H	3.010279	5.676002	1.501198
N	3.969311	4.590940	0.015997
C	5.852836	5.790321	2.298410
H	5.291823	6.439356	1.617326
H	6.595748	6.407567	2.814916
C	4.899449	5.137468	3.259173
C	4.560839	5.669568	4.494915
H	5.044494	6.579895	4.834640
C	3.598902	5.028238	5.277768
H	3.318184	5.429221	6.245975
C	3.009955	3.863021	4.786201
H	2.254515	3.330759	5.354372
C	3.402619	3.369602	3.549594
H	2.982585	2.463559	3.129192
N	4.338157	3.983698	2.785222
C	5.693020	0.905430	2.654579
H	6.461640	0.264782	3.104609
H	5.079704	0.332867	1.960603
H	5.056340	1.316620	3.438777
N	3.703995	1.945988	0.795873
N	2.562334	2.104688	0.457819
N	1.443954	2.199800	0.132609

References:

(1) Company, A.; Sabenya, G.; Gonzalez-Bejar, M.; Gomez, L.; Clemancey, M.; Blondin, G.; Jasniewski, A. J.; Puri, M.; Browne, W. R.; Latour, J. M.; Que, L., Jr.; Costas, M.; Perez-Prieto, J.; Lloret-Fillol, J. *J. Am. Chem. Soc.* **2014**, *136*, 4624.

(2) Ravel, B.; Newville, M. *J. Sync. Rad.* **2005**, *12*, 537.

(3) Newville, M. *J. Sync. Rad.* **2001**, *8*, 96.

(4) Rehr, J. J.; Albers, R. C. *Rev. Mod. Phys.* **2000**, *72*, 621.

(5) Martin-Diaconescu, V.; Bellucci, M.; Musiani, F.; Ciurli, S.; Maroney, M. J. *J. Biol. Inorg. Chem.* **2012**, *17*, 353.

(6) Zambelli, B.; Berardi, A.; Martin-Diaconescu, V.; Mazzei, L.; Musiani, F.; Maroney, M. J.; Ciurli, S. *J. Biol. Inorg. Chem.* **2014**, *19*, 319.

(7) Neese, F. *Wiley Interdisciplinary Reviews: Computational Molecular Science* **2012**, *2*, 73.

(8) Schäfer, A.; Horn, H.; Ahlrichs, R. *J. Chem. Phys.* **1992**, *97*, 2571.

(9) Weigend, F.; Ahlrichs, R. *Phys. Chem. Chem. Phys.* **2005**, *7*, 3297.

(10) Neese, F. *Inorg. Chim. Acta* **2002**, *337*, 181.

(11) Grimme, S.; Antony, J.; Ehrlich, S.; Krieg, H. *J. Chem. Phys.* **2010**, *132*.

(12) Grimme, S.; Ehrlich, S.; Goerigk, L. *J. Comp. Chem.* **2011**, *32*, 1456.

(13) Klamt, A.; Schuurmann, G. *J. Chem. Soc., Perkin Trans. 2* **1993**, 799.

(14) DeBeer George, S.; Petrenko, T.; Neese, F. *Inorg. Chim. Acta* **2008**, *361*, 965.

(15) DeBeer George, S.; Petrenko, T.; Neese, F. *J. Phys. Chem. A* **2008**, *112*, 12936.

(16) Nakamoto, K. *Infrared and Raman Spectra of Inorganic and Coordination Compounds. Part B: Application in Coordination, Organometallic, and Bioinorganic Chemistry, 5th Edition*; John Wiley & Sons, Inc.: Hoboken, New Jersey, 2009.